NAVAL POSTGRADUATE SCHOOL
MONTEREY, CALIFORNIA

THESIS

ESTIMATING THE ACOUSTIC MODAL ARRIVALS USING SIGNALS TRANSMITTED FROM TWO SOUND SOURCES TO A VERTICAL LINE HYDROPHONE ARRAY IN THE 1996 SHELFBREAK PRIMER EXPERIMENT

by

Christopher W. Miller

June, 1998

Thesis Advisor: Ching-Sang Chiu
Thesis Co-Advisor: Charles Therrien

Approved for public release; distribution is unlimited.

REPORT DOCUMENTATION PAGE

Form Approved OMB No. 0704-

1. AGENCY USE ONLY *(Leave blank)*	2. REPORT DATE	3. REPORT TYPE AND DATES COVERED
	June, 1998	Master's Thesis

4. TITLE AND SUBTITLE: ESTIMATING THE ACOUSTIC MODAL ARRIVALS USING SIGNALS TRANSMITTED FROM TWO SOUND SOURCES TO A VERTICAL LINE HYDROPHONE ARRAY IN THE 1996 SHELFBREAK PRIMER EXPERIMENT.

5. FUNDING NUMBERS

6. AUTHOR(S) Miller, Christopher W.

7. PERFORMING ORGANIZATION NAME(S) AND ADDRESS(ES)
Naval Postgraduate School
Monterey CA 93943-5000

8. PERFORMING ORGANIZATION REPORT NUMBER

9. SPONSORING/MONITORING AGENCY NAME(S) AND ADDRESS(ES)

10. SPONSORING/MONITORING AGENCY REPORT NUMBER

11. SUPPLEMENTARY NOTES: The views expressed in this thesis are those of the author and do not reflect the official policy or position of the Department of Defense or the U.S. Government.

12a. DISTRIBUTION/AVAILABILITY STATEMENT
Approved for public release; distribution is unlimited.

12b. DISTRIBUTION CODE

13. ABSTRACT *(maximum 200 words)* During the 1996 multi-institutional Shelfbreak PRIMER experiment, low frequency sound sources were moored on the continental slope south of Cape Cod. These sources transmitted phase encoded tomography signals which were monitored by vertical-line hydrophone arrays moored on the continental shelf. The measured signals were processed for the acoustic modal arrivals and their variability in time. The processing entailed pulse compression, coherent averaging, local sound-speed profile updates and an application of the Chiu-Miller-Lynch model-based modal beamforming technique. In this thesis, the signal processing procedure is discussed and the modal arrival estimates are examined. The model-based estimates are found to be of high quality, with all propagating modes individually resolved. This unambiguous separation of the high modes cannot be achieved using simple least-squares techniques because of under sampling. The temporal variability of the modal amplitudes and travel times are found to be related to ocean processes that are unique to the shelf-slope littoral environment.

14. SUBJECT TERMS	15. NUMBER OF PAGES
Modal Beamforming, Ocean-Acoustics, Signal Processing	36
	16. PRICE CODE

17. SECURITY CLASSIFICATION OF REPORT	18. SECURITY CLASSIFICATION OF THIS PAGE	19. SECURITY CLASSIFICATION OF ABSTRACT	20. LIMITATION OF ABSTRACT
Unclassified	Unclassified	Unclassified	UL

NSN 7540-01-280-5500

Standard Form 298 (Rev. 2-89)
Prescribed by ANSI Std. 239-18 298-102

Approved for public release; distribution is unlimited.

ESTIMATING THE ACOUSTIC MODAL ARRIVALS USING SIGNALS TRANSMITTED FROM TWO SOUND SOURCES TO A VERTICAL LINE HYDROPHONE ARRAY IN THE 1996 SHELFBREAK PRIMER EXPERIMENT

Christopher W. Miller

BSEL., California State Polytechnic University, 1991

Submitted in partial fulfillment
of the requirements for the degree of

MASTER OF SCIENCE IN ELECTRICAL ENGINEERING

from the

NAVAL POSTGRADUATE SCHOOL

June, 1998

Author: _____
Christopher W. Miller

Approved by: _____
Ching-Sang Chiu, Thesis Advisor

_____
Charles Therrien, Thesis Co-Advisor

_____
Herschel H. Loomis, Jr., Chairman
Department of Electrical and Computer Engineering

ABSTRACT

During the 1996 multi-institutional Shelfbreak PRIMER experiment, low frequency sound sources were moored on the continental slope south of Cape Cod. These sources transmitted phase encoded tomography signals which were monitored by vertical-line hydrophone arrays moored on the continental shelf. The measured signals were processed for the acoustic modal arrivals and their variability in time. The processing entailed pulse compression, coherent averaging, local sound-speed profile updates and an application of the Chiu-Miller-Lynch model-based modal beamforming technique. In this thesis, the signal processing procedure is discussed and the modal arrival estimates are examined. The model-based estimates are found to be of high quality, with all propagating modes individually resolved. This unambiguous separation of the high modes cannot be achieved using simple least-squares techniques because of under sampling. The temporal variability of the modal amplitudes and travel times are found to be related to ocean processes that are unique to the shelf-slope littoral environment.

TABLE OF CONTENTS

I. INTRODUCTION

A. THE SHELFBREAK PRIMER EXPERIMENT

The Shelfbreak PRIMER field study was a multi-institutional, joint effort by the Naval Postgraduate School (NPS), the Woods Hole Oceanographic Institution (WHOI), the University of Rhode Island, and Harvard University. As the oceanographic conditions at the shelfbreak differ drastically between seasons, the field work included two intensive three-week experiments, one in July 1996 (summer) and the other in February 1997 (winter). The acoustic goal was to understand the propagation of sound from the continental slope to the continental shelf, including the effects of shelfbreak frontal features. The oceanographic goal was to characterize the mean and seasonal changes of the ocean circulation and determine the kinematics and dynamics of the shelfbreak frontal processes. [Refs. 1-2]

The Shelfbreak PRIMER study area is shown in Figure 1. The area is south of Cape Cod in the vicinity of the continental shelfbreak. The experimental location

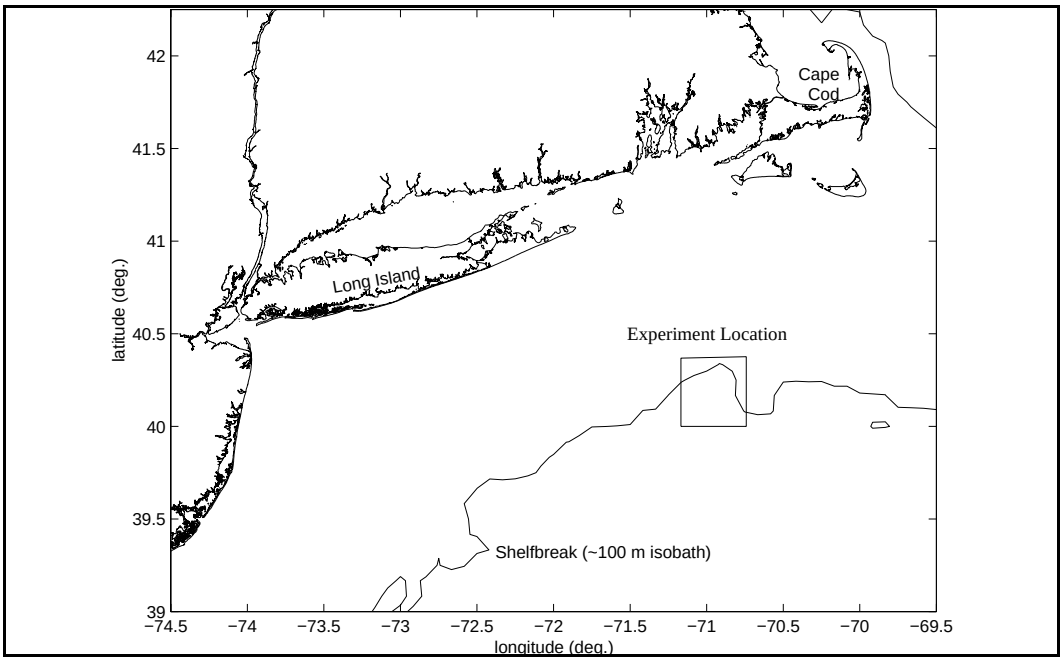

Figure 1. Geographic location of the 1996 Shelfbreak PRIMER experiment.

provided a complex coastal environment for studying sound propagation, from the continental slope to the continental shelf which is influenced by oceanographic and geological processes related to the shelfbreak. The shelf waters are cold and fresh, and vary considerably with season and location, while the warmer slope water is influenced by the Gulf Stream. The study area is marked by a significant ocean front at the shelf-break, the presence of strong internal tides, solitary waves (solitons), and complex flows, eddies and meanders [Refs. 1-4].

The Shelfbreak PRIMER field study was a cross-discipline physical oceanography and underwater acoustics experiment. In an effort to provide as much environmental data as possible a large suite of oceanographic and acoustic instruments were deployed. Figure 2 shows the principal acoustic moorings deployed during the summer experiment.

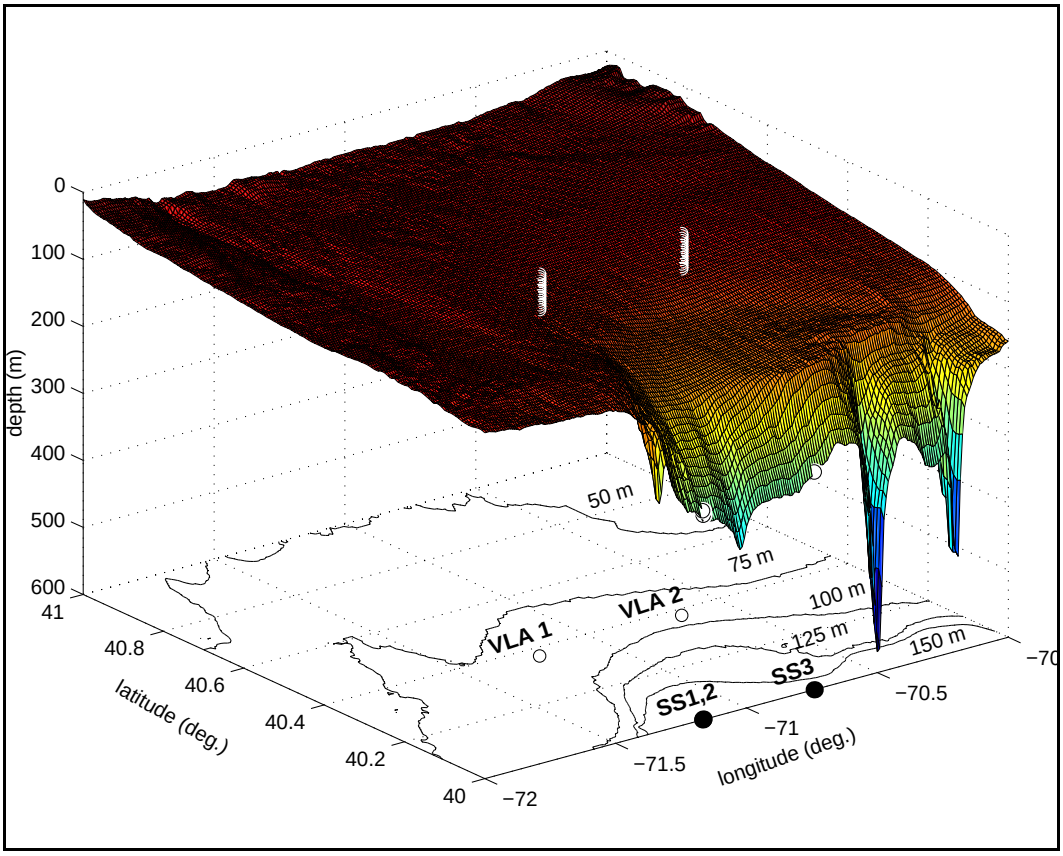

Figure 2. The mooring configuration of the Shelf-break PRIMER summer experiment. The VLA's (VLA1 and VLA2) were moored on the continental shelf, while the sound sources (SS1, SS2, and SS3) were moored on the slope. The highly variable bathymetry of the study area is also displayed.

The primary sensors for the acoustic component of the experiment were two vertical-line hydrophone arrays (VLA's). Each array consisted of 16 hydrophone elements that spanned the lower two-thirds of the water column. The emitters used for the experiment were one 224 Hz tomography source with a bandwidth of 32 Hz, and two 400 Hz tomography transceivers, each with a bandwidth of 100 Hz. This thesis study focused on the modal propagation along the western acoustic track. The transmitted signals from the 224 Hz (SS1), and 400 Hz (SS2) sources, co-located at the South-West corner, and received by the North-West vertical line array (VLA1) were processed and analyzed within the framework of acoustic normal mode theory. [Refs. 5-8]

B. THESIS OBJECTIVES, APPROACH, AND OUTLINE

The objective of this thesis is to (1) optimally process the acoustic VLA data for modal arrivals (magnitudes and travel times), and (2) relate the observed variability in the modal arrivals to oceanographic processes. The signal processing can be subdivided into pulse compression and coherent averaging (temporal processing), and modal beamforming (space-time processing). The transmitted signals were multiple periods of phase-modulated pseudo-random digits. A coherency study was performed to determine the optimal averaging time and optimum averaging gain. Once the individual hydrophone pulse arrival structures were processed, a model-based modal beamformer was applied to the data [Ref. 9], using updated sound-speed profiles local to the VLA. The variability analysis entailed examining the time series modal magnitude and travel time extracted from the modal-beamformed data.

The remainder of this thesis consists of three chapters. Chapter II describes the signal processing methods used to process the VLA hydrophone data for the modal arrival structure. Chapter III presents and discusses the data processing results, and discuses the observed acoustic variability in relation to the shelfbreak oceanographic processes. Chapter IV presents the conclusions of this study.

II. SIGNAL PROCESSING

A. PULSE COMPRESSION AND COHERENT AVERAGING

1. Source Signal Characteristics

The signal design and processing of ocean acoustic tomography has traditionally used the approach pioneered by T. Birdsall and K. Metzger. The Birdsall-Metzger method uses phase encoded periodic signals to eliminate self-clutter. These signals are easily generated and processed using digital techniques [Ref. 10, 11]. By modulating the signal's phase with a pseudo-random binary sequence, a deterministic narrow pulse can be realized upon matched filtering. The sequence can also be transmitted repeatedly to achieve additional signal processing gain at the receiver by averaging consecutive sequences.

Maximal-length binary sequences (m-sequences) have been used to generate a pseudo-random signal that can be decoded with no side-lobes in the time domain, provided that the sequence period is much greater than the arrival spread of the received signal [Ref. 12]. Figure 3 shows how the m-sequences are generated using linear shift register techniques. The shift register taps identify the sequence's "law" value, typically

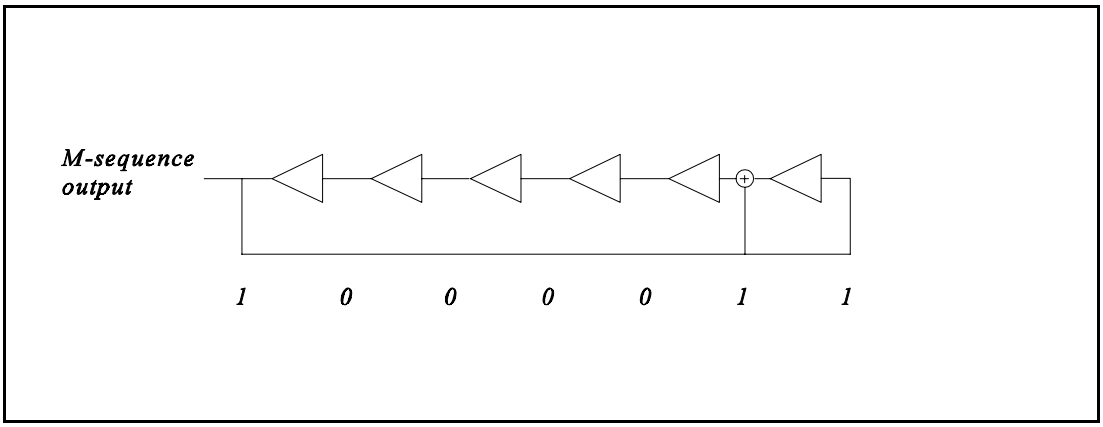

Figure 3. Shift register generation of the pseudo-random M-sequence with a law value of 103. This m-sequence was used in the 224 Hz sound source (SS1).

represented as an octal value, which defines the binary code [Ref. 13]. For the 224 Hz tomography source, SS1, the m-sequence law used was 103_8, or 1000011_2. The exact m-sequence generated for the experiment used an initial shift-register load of one. The same m-sequence (except for a time delay associate with a random seed of the shift register) would be generated with any random initial load, since an m-sequence is only determined by its law value. The source signal is generated by phase encoding the binary sequence to a suitable carrier for acoustic transmission, with each m-sequence digit encoded by a fixed number of carrier cycles. It is the number of carrier cycles per m-sequence digit that defines the temporal extent of the pulse of the output of a matched filter, which is the inverse of the modulating filter.

	SS1	SS2	SS3
Center Frequency, f_0	224 Hz	400 Hz	
Full Bandwidth	32 Hz	100 Hz	
m-sequence law (octal)	103	1533	1175
m-sequence length, L	63 digits	511 digits	
digit width (resolution)	14 cycles = 62.5 msec	4 cycles = 10 msec	
m-sequence period, T_s	3.9375 sec	5.11 sec	
m-sequences transmitted	30 sequences	48 sequences	
transmission length	118.125 sec	245.28 sec	

Table 1. Source Signal characteristics for pulse compression in Shelf-break PRIMER.

2. M-Sequence Period Mismatch

In most previous tomography experiments, the m-sequence transmissions were typically periodically averaged to reduce both the size of the data and to attain coherent averaging gain. The Shelfbreak PRIMER VLA1 sample rate was hardware configured to be 1395.0892 Hz (divided down from a 5 MHZ reference frequency). The non-integer sample rate introduced minor difficulties in the periodic averaging of the received signal

and in the construction of the matched filter. These difficulties as well as their solutions are discussed next.

The m-sequence period, T_s, of each transmitted signal is listed in Table 1. Since the VLA digitized the received signal at a non-integer sample rate, the period of the received m-sequence was always mismatched to that of the transmitted sequence due to the discrete nature of the digitization process. To illustrate this mismatch, let us use the 224 Hz transmission as an example. At a sampling frequency of 1395.089 Hz, the length of the received sequence is truncated to 5493 samples, while the true period length of the transmitted sequence is 5493.16406 samples. This mismatch represents a time skew of 117.6 µs per m-sequence. Since the source signal consists of thirty consecutive sequences in each transmission, a time-skew of 3.528 msec can be found over the transmission without compensating for this mismatch. For the 224 Hz signal, with a digit resolution of 62.5 ms, a skew of 3.5 ms is negligible. In contrast, the 400 Hz signal is much more sensitive to the mismatch, introducing a time skew much greater than the m-sequence digit width of 10 ms. This skew can cause severe degradation in the subsequent coherent averaging process without a proper correction. Errors introduced by the period mismatch without correction are summarized in Table 2.

	SS1	SS2	SS3
m-sequence length	5493.16406 samples	7128.90625 samples	
perceived length by VLA	5493 samples	7128 samples	
single m-sequence skew	117.6 µs/m-sequence	649.6 µs/m-sequence	
skew over one transmission of multiple sequences	3.528 msec	31.18 msec	

Table 2. Summary of error due to uncorrected period mismatch.

Since the skew is based solely on sample rate selection and signal period, it can easily be corrected by applying a phase shift of

$$\Delta\phi_p = j2\pi f\left(T_s - \frac{fix\,(T_s F_s)}{F_s}\right) \tag{2.1}$$

to each perceived period of the received sequences to re-align the received signal to that of the transmitted period. The 'fix' function used in Eq. 2.1 rounds the argument to the nearest integer, towards zero.

Figure 4 shows both the uncorrected and corrected demodulated envelopes of a received 400 Hz tomography signal containing 48 m-sequence periods. The uncorrected

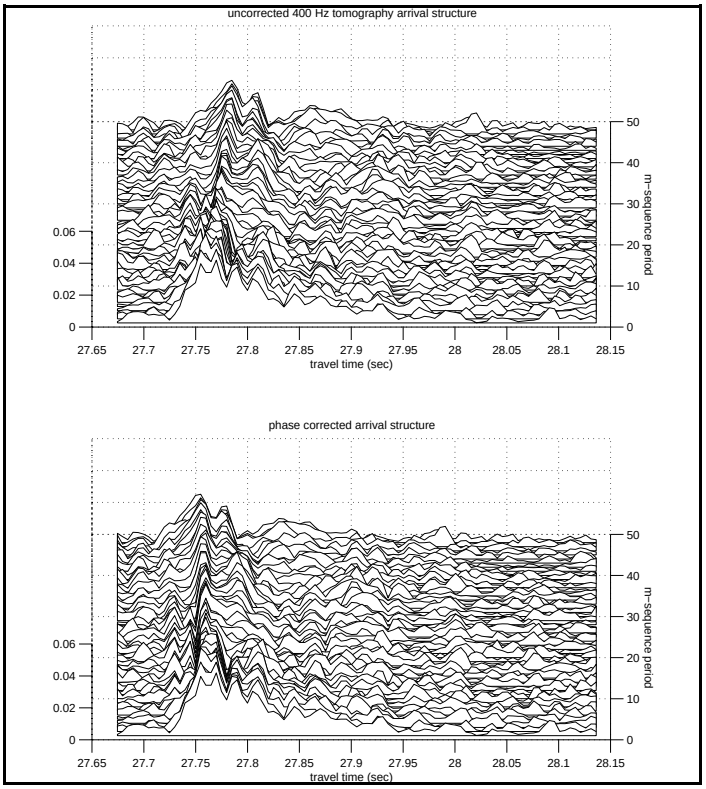

Figure 4. Uncorrected (top) and corrected (bottom) period-mismatched arrival structure of 48 consecutive m-sequences in a single 400 Hz transmission for the 1996 year-day 206.3231.

pulse arrival structure (top panel) shows a clear time skew that can severely degrade coherent averaging gain without compensation.

3. Coherent Averaging

The ocean environment is highly variable at the New England continental shelf, particularly in the vicinity of the shelfbreak. The ocean variability caused significant signal fluctuations during the course of the Shelfbreak PRIMER experiment; this variability has limited how many arrival structures could be coherently averaged to attain the maximum averaging gain. The time duration over which one can coherently average multiple arrival structures to increase the signal-to-noise ratio before signal saturation or degradation occurs can be thought of as the inherent coherency time of the ocean sound channel.

A temporal coherency study was performed over a transmission series to

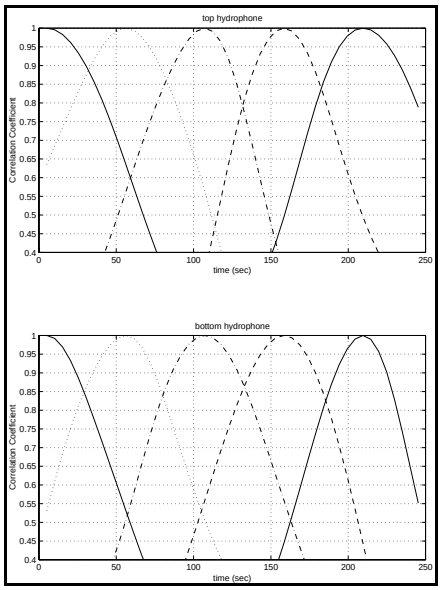

Figure 5. The cross-correlation coefficients of the 400 Hz pulse responses measured at different times with five reference responses.

determine the maximum number of arrival structures that could be coherently averaged before degradation in the pulse resolution was seen in the arrival structure. The coherency time can be estimated by cross-correlating the arrival structures, i.e., pulse responses, observed at different times with one at a reference time. Figure 5 shows the correlation results for both the top and bottom hydrophone arrivals for the 400 Hz signal. Different reference times were used to study the stationarity of the coherence.

Defining the limiting correlation value, below which the signal decorrelates significantly, to be 0.5 a coherence time of approximately 60 seconds is observed. This coherence time is consistent with that estimated by Chiu, et. al. [Ref. 4] based on a computer modeling study accounting for the effects due to large scale amplitude internal waves which have been observed frequently in the same geographic area. Note that the coherence time is not exactly depth independent and stationary, but exhibits small variations.

Further investigation was performed by analyzing the signal-to-noise ratio (SNR) of the cumulative coherent averages of a transmission. Figure 6 shows the cumulative coherently averaged arrival structures for a 400 Hz tomography signal. The signal power was calculated over the predicted signal multi-path spread which occupies the time interval from 27.56 to 28.7 seconds relative to the beginning of the signal's transmission. The noise power was calculated over the tail of the arrival structure segment, between 28.85 to 32.53 seconds. This SNR value was calculated for the first arrival structure, the coherent average of the first two arrival structures, and so on, up to the coherent average of 48 consecutive arrival structures. The theoretical coherent averaging gain in a static sound channel is 10log(N), where N is the number of pulse responses being averaged. It is expected that the experimental result should approximate this theoretical gain as long as the ocean sound channel remains coherent. Figure 6 shows the experimental SNR gain and how it compares to the theoretical gain. The measured SNR gain shows a saturation at approximately 50 seconds, which is consistent with the results of the cross-correlation analysis. Figure 7 shows the cumulative coherently averaged pulse arrival structures as a function of the averaging time.

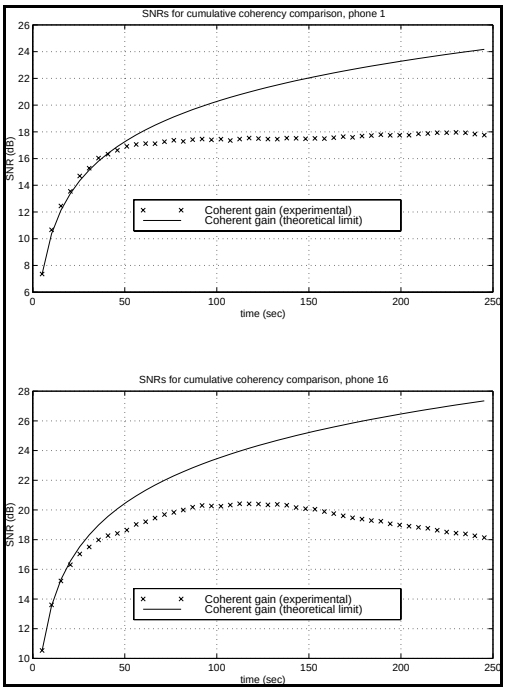

Figure 6. Experimental vs. Theoretical gain (SNR) for the 400 Hz cumulative coherent averaged pulse responses for the top and bottom hydrophones of the VLA.

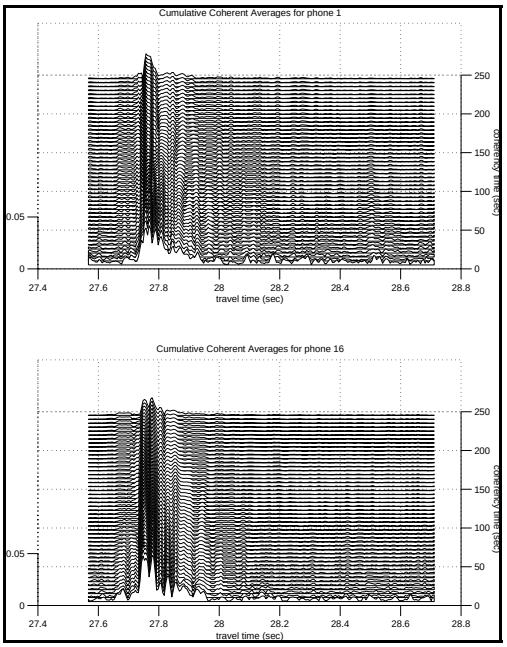

Figure 7. Cumulative coherent averaged 400 Hz pulse arrival structures shown vs. the averaging time for the top and bottom VLA hydrophones.

It is important to note that although the SNR gain saturates beyond 50 seconds (10 pulse responses) of coherent averaging, the individual pulses actually degrade beyond that. This implies that the number of pulse responses that can be coherently averaged before loss of pulse integrity is limited to ten.

B. MODEL-BASED MODAL BEAMFORMING

The ability to separate the vertical sound-field structure into individual normal modes for the purpose of ocean acoustic tomography has been demonstrated using an iterative model-based modal beamformer [Ref. 9]. This same technique was used to perform modal beamforming on the m-sequence removed, coherently averaged pulse responses measured by the North-West vertical line array, VLA1. For completeness this

technique will be outlined next.

Computed by solving the Helmholtz Equation, the orthogonal normal modes can be fitted to the measured vertical sound pressure field at the hydrophone array to obtain their coefficients. With a continuous line array, the orthogonality of the modes is guaranteed. In practice, deployable arrays can't span the entire water column due to fishing activity, hardware and environmental restrictions. Another limiting factor is hydrophone spacing. Without densely populated hydrophone elements, one ends up with an under-sampled pressure field. This under-sampling destroys the exactness of the orthogonality, which can result in mode-filter leakage of energy from one mode to another. [Ref. 9]

The complex envelope of sound pressure $p(z_k,t_m)$ sampled by each hydrophone in a VLA is related to the baseband pressure spectrum $P(z_k,f_j)$ via a Fourier transform:

$$P(z_k,f_j)=\sum_{m=0}^{M-1} p(z_k,t_m)\ e^{(-j2\pi f_j t_m)}\Delta t. \qquad (2.2)$$
$$k=1,2,3,...,K$$
$$f_j=\frac{j}{M\Delta t}$$
$$j=-\frac{M}{2}+1,-\frac{M}{2}+2,...,+\frac{M}{2}$$
$$t_m=t_0+m\Delta t$$

where z_k is the depth of the k^{th} hydrophone in the VLA, t_m denotes the discrete times at which the arrival structure is sampled, Δt is the sampling interval and the f_js are the baseband frequencies with f_0=0 Hz. The interval MΔt defines an M-point time segment stretching the duration of the arrival structure that begins after time t_0. According to full-wave theory, these baseband spectra, $P(z_k,f_j)$, can be expressed as a linear combination of normal modes sampled at the different hydrophone depths. Accounting for the contamination by additive noise and denoting the sound pressure spectrum of the

complex envelope of noise at each phone by $N(z_k,f_j)$, the measured spectra can be expressed as

$$P(z_k,\ f_j)=\sum_{n=1}^{N} A_n(f_j)Z_n(z_k,\ f_j+F_c)+N(z_k,\ f_j)\ .$$
$$k=1,2,3,...,K \qquad (2.3)$$
$$j=-\frac{M}{2}+1,-\frac{M}{2}+2,...,+\frac{M}{2}$$

where N is the number of modes to be used in the beamforming and F_c is the carrier or center frequency of the transmitted bandpass signal. Weighted by their frequency dependent coefficients A_n in the sum, the local normal modes Z_n are functions of both depth, z, and frequency, $f=f_c+f_j$, that satisfy the following governing equation and boundary conditions:

$$\left(\frac{d^2}{dz^2}-\frac{1}{\rho(z)}\frac{d\rho(z)}{dz}\frac{d}{dz}+\left[\frac{2\pi f}{c(z)}\right]^2-k_n(f)^2\right)Z_n(z,\ f)=0\ .$$
$$Z_n(0,\ f)=0$$
$$Z_n(h_i^-,\ f)=Z_n(h_i^+,\ f), \qquad i=1,2,...,I \qquad (2.4)$$
$$\frac{1}{\rho(h_i^-)}\frac{d}{dz}\ Z_n(h_i^-,\ f)=\frac{1}{\rho(h_i^+)}\frac{d}{dz}\ Z_n(h_i^+,\ f), \qquad i=1,2,...,I$$
$$\frac{d}{dz}\ Z_n(h,\ f)=0.$$

Additionally, the mode functions at each frequency possess the property of orthogonality:

$$\int_0^h \frac{1}{\rho(z)}\ Z_n(z,\ f)\ Z_m(z,\ f)\ dz\ =\ \delta_{n,m}\ . \qquad (2.5)$$

In Eq. 2.4, k_n is the horizontal wave number (or eigenvalue) of the nth mode, h is the total thickness of the acoustic waveguide that contains a total number of internal interfaces, h_i is the depth of the i^{th} interface (with i=1 denoting the sea floor and i>1 denoting the sediment-sediment interfaces below), and superscripts $^+$ and $^-$ denote depths just below

and above h_i, respectively. Given the sound-speed profile $c(z)$, density profile $\rho(z)$, and the depths of the water-sediment and sediment-sediment interfaces at the VLA location, the local normal modes and their eigenvalues can be determined by solving Eq. 2.4 and normalized using Eq 2.5. [Ref. 9, 14]

Once the normal mode functions are known and the time series measured by the VLA have been converted to baseband spectra, the major task in model based modal beamforming is to estimate the complex modal amplitudes A_n (i.e., the weighting coefficients) in the presence of "noise." Depending on the number of modes that are processed for, the meaning of noise shall be expanded to include model error, i.e., the signals in the higher modes that are not included. Once an estimate $\hat{A}_n(f_j)$ of $A_n(f_j)$ is obtained, an estimate $\hat{a}_n(t_m)$ of the modal arrival structure $a_n(t_m)$ in time can be constructed using an inverse Fourier transform

$$\hat{a}_n(t_m) = \sum_{j=-\frac{M}{2}+1}^{+\frac{M}{2}} \hat{A}_n(f_j)\, e^{(+j2\pi f_j t_m)} \Delta f . \qquad (2.6)$$
$$m = 0,1,2,\ldots,M-1,$$
$$\Delta f = \frac{1}{M\Delta t}$$

To ensure that the mode beamformer is computationally tractable, even for large bandwidth signals, Chiu *et al.*[Ref. 9] formulated a procedure that operates on the baseband spectral data one frequency at a time. The measurement equation (Eq. 2.3) at each baseband frequency, f_j, can be rewritten in matrix-vector notation as

$$\boldsymbol{P}_j = \boldsymbol{Z}_j \boldsymbol{A}_j + \boldsymbol{N}_j \qquad (2.7)$$

where the subscript "j" is used to denote quantities associated with the baseband frequency f_j. Associating Eq. 2.7 with Eq. 2.3; $\boldsymbol{P}_j$ is identified as a column vector of length K, containing the measured spectral values of the complex envelopes of sound pressure at each of the hydrophone depths, $\mathbf{Z}_j$ is a K x N "mode shape" matrix, whose

columns are the "mode vectors," each containing the depth samples of a specific mode function evaluated at the hydrophone depths, $\boldsymbol{A}_j$ is a column vector of length N denoting the unknown complex modal amplitudes A_n at frequency j, and $\boldsymbol{N}_j$ is a column vector of length K representing additive noise.

The "best" estimate $\hat{\boldsymbol{A}}_j$ of $\boldsymbol{A}_j$ may be defined as the one that has the least mean square error and is linear with the data $\boldsymbol{P}_j$, i.e.,

$$\hat{\boldsymbol{A}}_j = \boldsymbol{O}_j \boldsymbol{P}_j . \tag{2.8}$$

Under the assumption that second moment statistical models for $\boldsymbol{A}_j$ and $\boldsymbol{P}_j$ are available, the Gauss-Markov theorem asserts that such an estimate is unique and that the corresponding estimator, for linear observations, is given by

$$\begin{aligned} \boldsymbol{O}_j &= \langle \boldsymbol{A}_j \boldsymbol{A}_j^{\boldsymbol{T}} \rangle \boldsymbol{Z}_j^{\boldsymbol{T}} (\boldsymbol{Z}_j \langle \boldsymbol{A}_j \boldsymbol{A}_j^{\boldsymbol{T}} \rangle \boldsymbol{Z}_j^{\boldsymbol{T}} + \langle \boldsymbol{N}_j \boldsymbol{N}_J^{\boldsymbol{T}} \rangle)^{-1} \\ \textit{or} & \\ \boldsymbol{O}_j &= (\langle \boldsymbol{A}_j \boldsymbol{A}_j^{\boldsymbol{T}} \rangle^{-1} + \boldsymbol{Z}_j^{\boldsymbol{T}} \langle \boldsymbol{N}_j \boldsymbol{N}_j^{\boldsymbol{T}} \rangle^{-1} \boldsymbol{Z}_j)^{-1} \boldsymbol{Z}_j^{\boldsymbol{T}} \langle \boldsymbol{N}_j \boldsymbol{N}_j^{\boldsymbol{T}} \rangle^{-1} . \end{aligned} \tag{2.9}$$

where the brackets <•••> denote the expected value or first moment statistics.
The corresponding error covariance matrix of the solution can be expressed as

$$\langle (\hat{\boldsymbol{A}}_j - \boldsymbol{A}_j)(\hat{\boldsymbol{A}}_j - \boldsymbol{A}_j)^T \rangle = \langle \boldsymbol{A}_j \boldsymbol{A}_j^{\boldsymbol{T}} \rangle - \boldsymbol{O}_j (\langle \boldsymbol{A}_j \boldsymbol{A}_j^{\boldsymbol{T}} \rangle \boldsymbol{Z}_j^{\boldsymbol{T}})^T . \tag{2.10}$$ [Ref. 9]

The Gauss-Markov estimator allows for an *a priori* solution covariance, $\langle \boldsymbol{A}_j \boldsymbol{A}_j^{T} \rangle$. It is through this covariance that one can inject additional constraints, obtained by propagation modeling, using basic environmental information, to improve the beamformer results. For example, with sufficient environmental information (i.e., sound speed, bottom density, surface roughness, etc.) a propagation model can estimate the received modal amplitudes and the time spread between the propagating modes. Given an adequate model prediction $\overline{\overline{A_n}}(f_j)$, of the complex modal amplitudes $A_n(f_j)$, we can express their relationship by

$$A_N(f_j) = G_n(f_j)\, e^{-j2\pi f_j \delta t_n}\, \overline{\overline{A_n}}(f_j)\,, \tag{2.11}$$

where $G_n(f_j)$ corresponds to a distortion and δt_n a translation [Ref. 9].

We can calculate a model for the solution covariance (Eq. 2.14) if we apply the following assumptions:

1. Translation and distortion of the predicted modal arrival structure are statistically independent. This is true if the dominant ocean processes that cause translation are different from those causing the distortion (i.e., processes of different time scales).
2. Both distortion and translation of the arrival structure of different modes are statistically independent. This assumption is, in general, inexact because different modes do not traverse non-overlapping sections of the water column, but is not a poor assumption when exact knowledge of such correlations are absent.
3. The second moments of the modal distortion factors are given by where the ϵ_n's are the modal-energy mismatch parameters. When ϵ_n=0, the ensemble average of the energy levels of the actual modal arrivals is identical to the predicted energy level. As ϵ_n deviates from zero, the predicted and the ensemble averaged levels become dissimilar.
4. The time translations have Gaussian statistics such that their probability density functions are given by

$$p(\delta t_n) = \frac{1}{\sqrt{2\pi}\sigma_{t_n}}\; e^{\frac{-\delta t_n^2}{2\sigma_{t_n}^2}}\,, \tag{2.13}$$

where σ_{t_n} is the standard deviation of the arrival time of mode *n* from that predicted by the model. [Ref. 9]

$$<A_n(f_j)A_m^*(f_j)> = \begin{cases} (1+\epsilon_n^2)\overline{\overline{A}}_n(f_j)\overline{\overline{A}}_n^*(f_j), & m=n \\ \exp[-(2\pi f_j)^2\dfrac{(\sigma_{t_n}^2+\sigma_{t_m}^2)}{2}]\overline{\overline{A}}_n(f_j)\overline{\overline{A}}_m^*(f_j), & m\neq n \end{cases} \quad (2.14)$$

This analytic covariance model contains statistical parameters for mode arrival time changes, and mode amplitude variations. The refinement of these statistical parameters along with the updated predictions of A_n (from previous iterations) is key to achieving improved mode beamformer performance. If the complex modal amplitudes predicted by the model are explicitly written out (Eq. 2.15) in terms of amplitude and arrival time, $\overline{\overline{t}}_n$, we can gain some insight into the type of additional constraints that are

$$\overline{\overline{A}}_n(f_j) = \overline{\overline{B}}_n(f_j)e^{-i2\pi f_j\overline{\overline{t}}_n} \quad (2.15)$$

being applied to this model-based modal beamformer. It follows from Eqs. 2.14 and 2.15, that

$$<A_n(f_j)A_m^*(f_j)> = e^{-(2\pi f_j)^2\frac{(\sigma_{t_n}^2+\sigma_{t_m}^2)}{2}}\overline{\overline{B}}_n(f_j)\overline{\overline{B}}_m^*(f_j)e^{-i2\pi f_j(\overline{\overline{t}}_n-\overline{\overline{t}}_m)}, \quad m\neq n\,. \quad (2.16)$$

Equation 2.16 reveals that the additional information contains the predicted relative arrival times $(\overline{\overline{t}}_n-\overline{\overline{t}}_m)$ between the different modes as well as the uncertainty of this information. The uncertainty placed on the relative arrival time information is imposed as the expected variance of the predicted arrival time. It is important to note that no constraints have been placed on the absolute arrival times. If constraints were placed on the absolute travel times that were too stringent, any error between the modeled anchor positions and the actual experimental configuration would result in significant error in the modeformed arrival structures. [Ref. 9]

C. SOUND SPEED PROFILE UPDATES

The estimation of the modal amplitudes (i.e., modal coefficients) requires that the normal modes at the location of the VLA be known. These normal modes depend strongly on the local sound speed profile. Because of the complex ocean processes associated with the shelfbreak, such as frontal meandering, eddy activities, internal tides, and solitary internal waves, the sound speed profile and hence the normal modes themselves are extremely dynamic with strong spatial and temporal changes. One can no longer afford to use a nominal sound speed profile to compute the normal modes and assume that the normal modes are static throughout the experiment. Such an assumption can result in a wrong set of normal modes for a given time, which when used for the modal beamforming can cause large modal sidelobes, making it difficult to resolve the individual modes.

In order to account for the dynamics of the normal modes at VLA1, we must obtain an accurate description of the sound speed profile as a function of both depth and time. This description was accomplished using the temperature time series obtained by four Brankner thermistor pods mounted at four depths, 24, 30, 50, and 70 m on VLA1, as well as salinity-temperature-depth data sampled by a surveying SeaSoar. A SeaSoar is a towed oceanographic sensor moving up and down the water column, with the horizontal resolution determined by the towing speed. The underlying logic was that the Brankner measurements contain information on the temporal evolution, while the SeaSoar data contain information on the vertical structure of the ocean's temperature.

SeaSoar data sampled near VLA1 were first extracted to construct the local vertical structure of the ocean temperature using an empirical orthogonal mode (EOF) analysis [Ref. 14]. The Brankner temperature time series were then projected onto the EOFs and their temporal variations are shown in Figure 8. Finally, the analyzed temperature profiles were converted into sound speed profiles using a standard empirical formula to facilitate an update, i.e. a recomputation, of the normal modes at each transmission time.

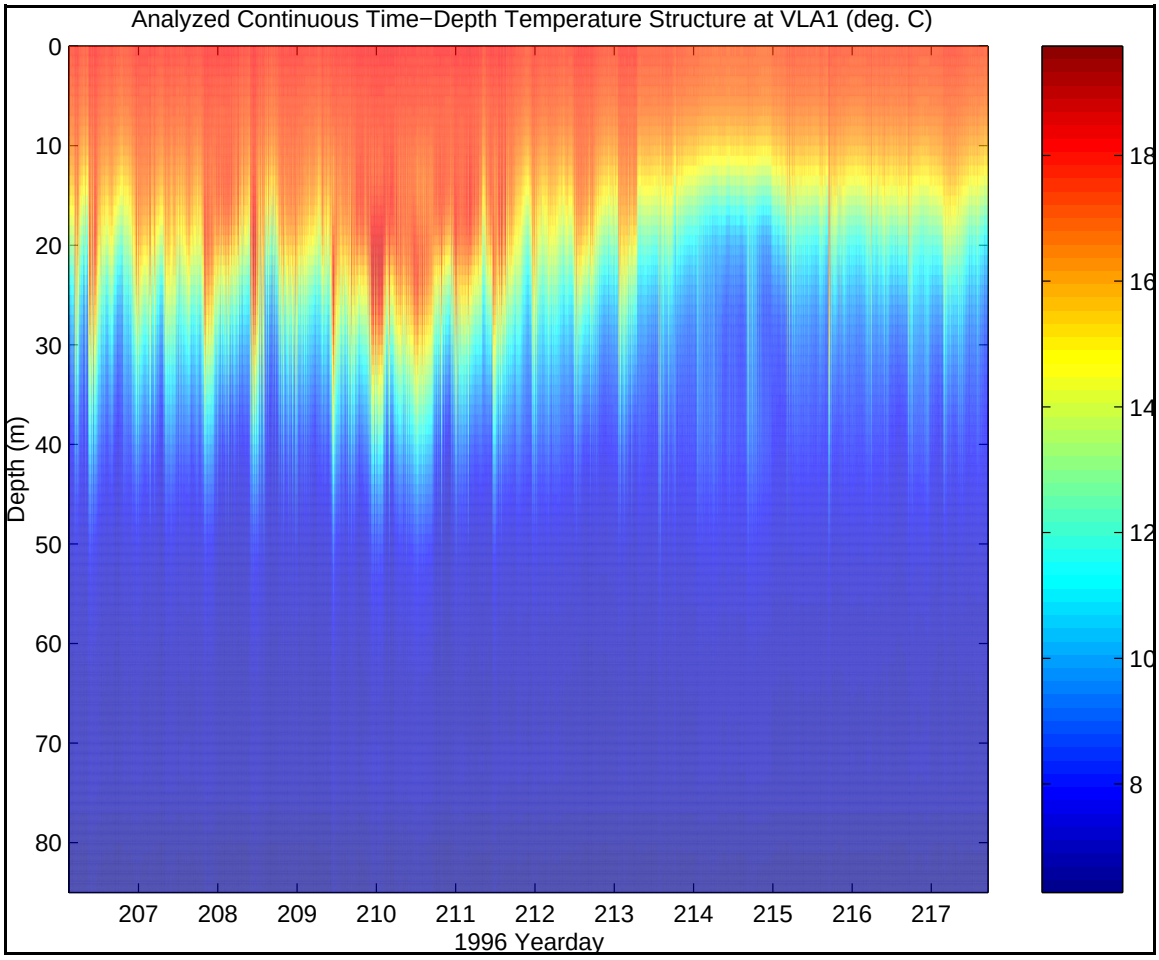

Figure 8. The temporal evolution and spatial changes of the temperature profile at the VLA1 site. This continuous ocean temperature field was analyzed from data sampled by four Brankner temperature pods and a surveying SeaSoar vehicle.

III. RESULTS AND DISCUSSION

A. MODAL ARRIVAL ESTIMATES

The Northwest vertical-line hydrophone array (VLA1) collected acoustic data between 24 July (yearday 206) and 2 August (yearday 215), 1996. During this time the Southwest 224 Hz tomography source (SS1) transmitted a phase-encoded signal every five minutes, while the Southwest 400 Hz source (SS2) transmitted every fifteen minutes. The sampling done by VLA1 has two time gaps during the entire experiment. These gaps in the data time series were caused by hardware problems; a blown fuse caused a twenty hours of data to be lost, and a disk drive problem caused another nine hours of data loss. Another 18-hour gap can be found in the modal beamforming results between 1996 yearday 209.6 to 210.4. During this time period, the sampling rate of VLA1 was increased to accommodate the broadband, explosive charge experiment which was another component of the PRIMER experiment. This higher rate data has not been beamformed at this time.

There are nine propagating modes at 224 Hz and 17 propagating modes at 400 Hz at the VLA1 location. The model-based mode beamformer was applied to the pulse arrival structures measured by the 16 omni-directional hydrophones of the VLA to estimate the variability of the amplitudes and travel times of these propagating modes. To demonstrate the improvement in quality of the model-based results, a simple least-squares solution [Refs. 15, 16] to Equation 2.7 was also computed to establish a baseline for comparison. The estimated modal arrivals constitute a fundamental data set for an inverse mapping of the coastal ocean temperature [Ref. 17]. The inversion of the travel times is known as tomography, a subject beyond the scope of this thesis research. Hereafter, the simple least-squares method will be referred as LS, whereas the model-based method will be referred as MB. The LS method can be interpreted as one without the time-separation and amplitude constraints provided initially by the model-based

procedure described in the previous chapter.

Figure 9 shows the arrival structures of the lowest mode (i.e., Mode 1) estimated by MB for both the 224 Hz and 400 Hz signals. When compared to the LS estimates displayed in Figure 10, it is evident that the MB estimate is of higher quality, particularly

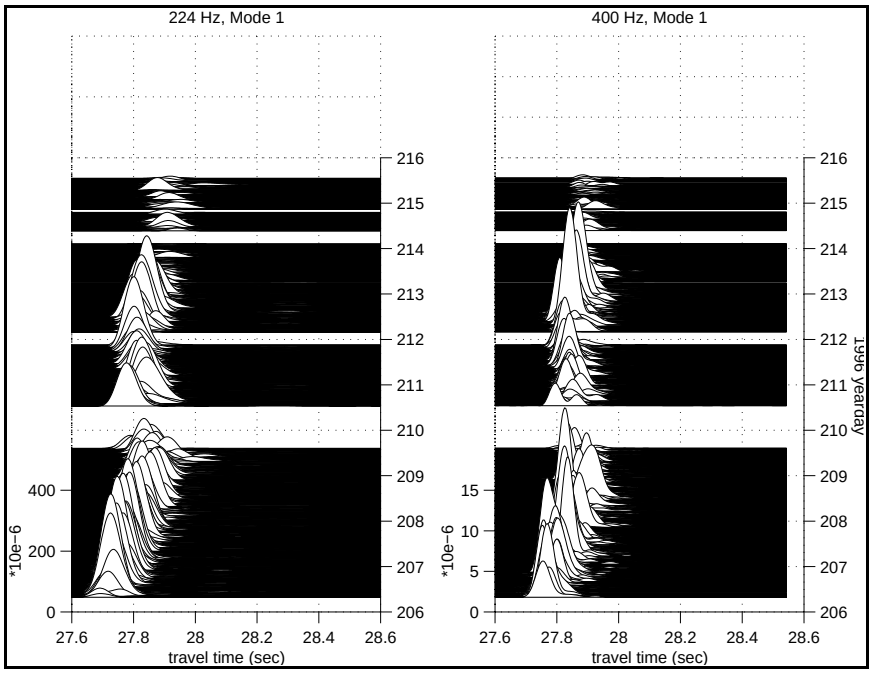

Figure 9. The arrival structure of Mode 1 estimated by the model-based beamformer as a function of transmission time for both the 224 Hz (left panel) and 400 Hz (right panel) signals.

for the 400 Hz signal. The modal sidelobes in the LS estimate for the 400 Hz signal are significant, resulting in multiple peaks, thus making the identification of the modal travel time ambiguous. The arrival structure estimated by MB is unimodal for each transmission.

The modal sidelobes are more severe for the higher order modes in the LS estimate. To illustrate this, we use the estimated arrival structure of Mode 16 for the 400 Hz transmissions as an example. The right panel of Figure 11 shows the LS estimate of the Mode 16 arrival structure. It is obvious that this higher mode is unresolved by LS because of the contamination or ambiguity presented by the severe sidelobes. The presence of modal sidelobes is inherent to spatial under sampling, inadequate hydrophone

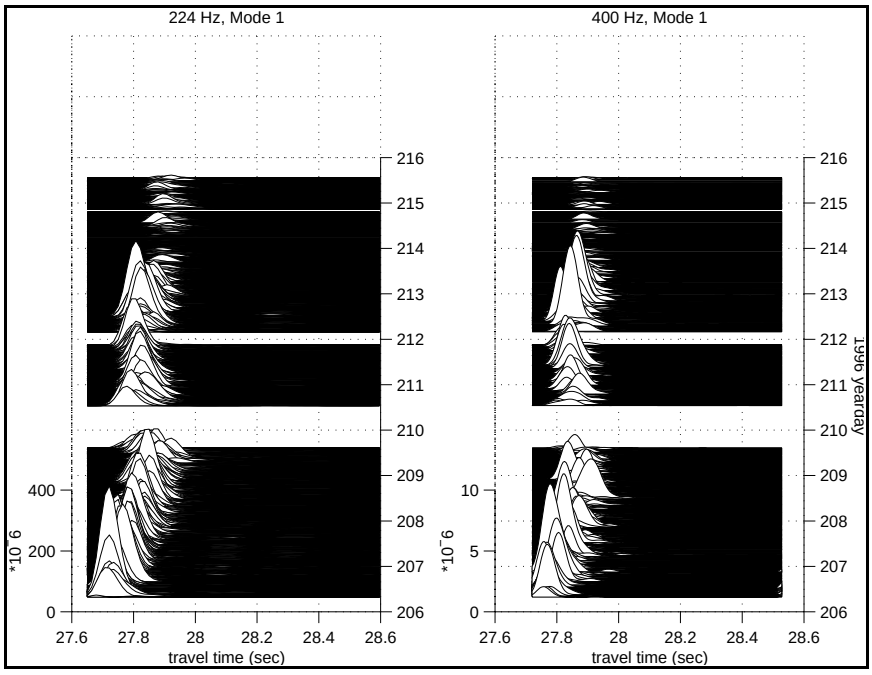

Figure 10. The arrival structure of Mode 1 estimated by simple least squares as a function of transmission time for both the 224 Hz (left panel) and 400 Hz (right panel) signals.

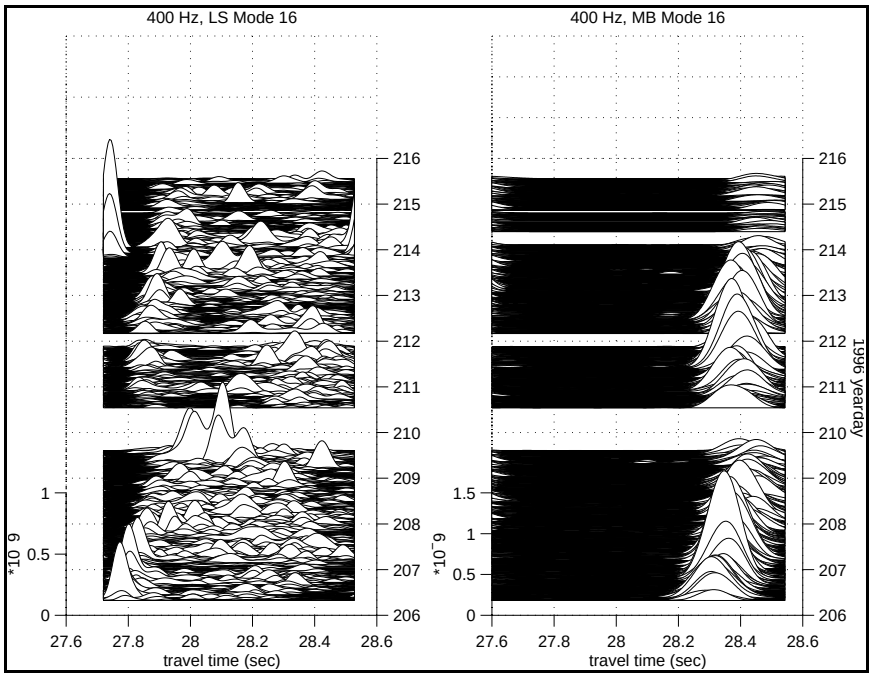

Figure 11. The arrival structure of Mode 16 estimated by simple least squares (left panel) and model based modal beamforming (right panel) for the 400 Hz signal.

spacing and aperture coverage of the water column. Higher modes and higher frequency energy are more affected by these sidelobes due to their shorter vertical wavelength and larger vertical span. The reduction of these sidelobes requires additional information, which can come from physical constraints that are meaningful, reasonable and refineable. This is the basic philosophy behind the MB method developed by Chiu *et al*. [Ref. 9], with progressive refinements based on the actual data. The right panel of Figure 11 shows the MB estimate of a clearly resolved Mode 16.

B. ACOUSTIC VARIABILITY

As seen in figures 9, 10, and 11, both the magnitude and travel time of the individual normal modes can vary significantly over time. This acoustic variability consists of many time scales, from weeks to minutes, and is mode-number dependent. Due to the high-resolution oceanographic data available during the experimental period, a fairly good estimate of the environmental influences that caused this variability can be developed.

On the close-to-weekly time scale, one can easily observe significant magnitude and travel time changes in the modal arrivals over all the modes, though they are much more apparent in the lower modes [Fig. 9]. The magnitude and travel time changes are well correlated; as the travel time increases, so does the magnitude of the pulse arrival. An increase in the travel time corresponds to an increase in the temperature along the transmission path. The key to understanding these results lies in the following questions: where along the path was the temperature increase, what caused the temperature to change, and why was the signal level affected? The SeaSoar, moored thermistors and infra-red satellite imagery provided the data needed to answer these questions. These oceanographic data show that there was a warm water filament that intruded over the transmission path twice over the course of the experiment. This warm filament was the remnant of a dissipated Gulf Stream, warm core ring. The core of the warm intrusions were isolated to the lower portion of the water column, and thus increased the sound

speed near the bottom. This sound speed increase resulted in a more upward-refracting sound channel, which reduced the signal attenuation due to bottom interactions (sediment absorption). After yearday 213, the warm filament dissipated and the lower water column on the shelf remained cold, and a much lower signal level is observed as a result of the much stronger interactions with the bottom. In general, the lower mode signal responses tend to be stronger because of the lesser bottom interactions.

The arrival times of the individual modes and their variations over transmission time for both the 224 and 400 Hz signals were extracted by picking the peaks of the MB estimates. The resulting time series of modal travel times are shown in Figure 12. Low pass filtering was applied to remove random fluctuations due to internal waves with periods shorter than three hours. The observed travel times show that the low modes

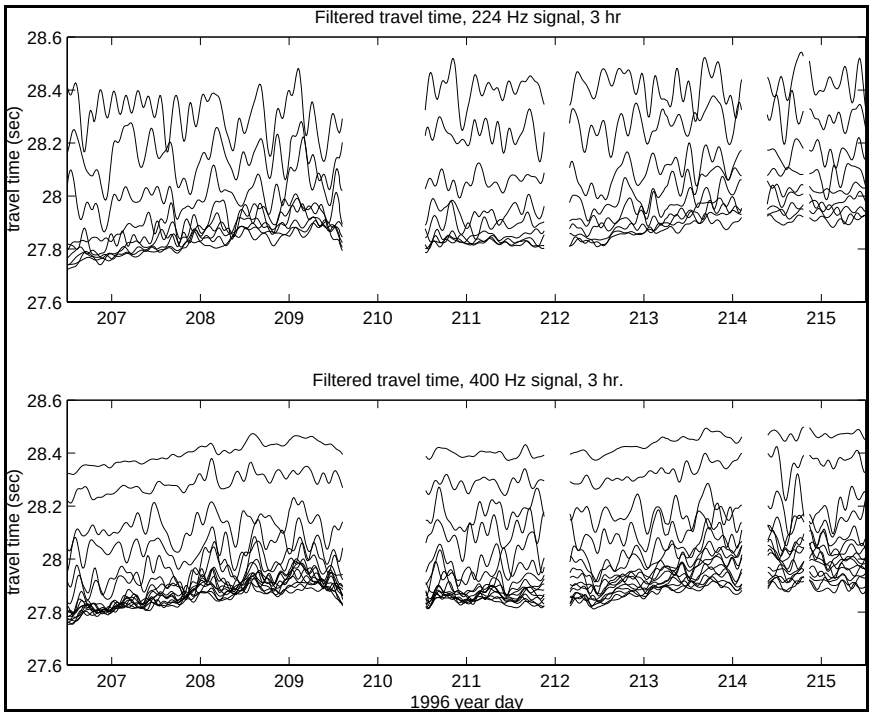

Figure 12. Measured variability of the normal mode travel times over the duration of the summer experiment. There are nine time series plotted in the top panel, each corresponds to one of the nine propagating modes at 224 Hz. There are 16 time series plotted in the bottom panel, each corresponds to a propagating mode at 400 Hz. The lower modes arrived sooner whereas the higher modes arrived later for both frequencies.

travel faster, and the higher modes travel slower. This result is expected in a shallow-water environment where the vertical extent of a mode increases with mode number. Higher modes are analogous to rays with steeper angles which travel through longer "raypaths" to reach the receiver.

In addition to the weekly variability introduced by the intrusion of the warm filament, other significant acoustic fluctuations with periods less than a day can also be observed [Fig. 12]. Fluctuations due to internal, diurnal tides are dominant in the intermediate modes for the 400 Hz and in the higher modes at 224 Hz. These modes have a large expression in the main thermocline where the internal tidal energy is mostly confined. At shorter time scales of several hours, the acoustic fluctuations can be attributed to longer-period internal waves as well as the large-amplitude internal soliton wavepackets [Ref. 3].

IV. CONCLUSIONS

A. SUMMARY OF FINDINGS

In this study, the model-based modal beamforming technique was applied to data recorded by a vertical line array (VLA) to estimate the arrival structure of the individual normal modes that propagated from the continental slope, through a shelfbreak front, to the continental shelf. The model-based estimate, when compared to a standard least-squares estimate, shows significant improvement. The improvements in the model-based estimate, in terms of filter resolution or sidelobes, are clearly seen for the higher modes. These modes are largely unresolved in the standard least-square estimate, while they are unambiguously resolved and identified in the model-based estimate. This results in a high quality data set of modal travel times to facilitate subsequent tomographic inverse analysis [Ref. 17].

Incorporation of the temporal changes of the normal modes was also found to be extremely important to maximizing the quality of the mode beamformer. This was accomplished by updating the sound speed profile based on an optimal interpolation analysis of the in-situ temperatures measured in the vicinity of the VLA. This update was then followed by re-computing the normal modes for each transmission time.

An empirical study of the coherence time of this shelf-slope sound channel at the Shelfbreak PRIMER transmission frequencies was carried out to investigate how long the signal can be coherently averaged before saturation or degradation occurs. Based on data obtained by the top and bottom hydrophones of the VLA, this coherence time was estimated to be approximately 50 s, although mild nonstationarity and inhomogeneity were observed. This coherence time was used to determine the number of consecutive pulse responses that could be coherently averaged to maximize the SNR without spreading the response structure.

A first look at the variability of the acoustic normal modes was taken using the

estimated modal arrival structure in conjunction with a high-resolution oceanographic data set. Significant fluctuations in modal travel times and magnitudes were found in multiple time scales due to oceanographic processes of different types such as warm-ring filament intrusions, internal tides, and internal waves. An in-depth study of the dynamics of these ocean processes and a quantification of their influences on the acoustic transmissions are currently going on.

B. RECOMMENDATIONS FOR IMPROVEMENT

Several improvements of the signal processing of the Shelfbreak PRIMER acoustic data are recommended. First, the bandwidth of the 400 Hz signal was 100 Hz. However, because of the model-based technique was developed only for narrow-band signals, only a sub-band of 32 Hz was processed. There are two options to proceed. One option is to modify the modal beamforming method to accommodate for the 100 Hz bandwidth. This can be accomplished by dividing the 100 Hz band into several narrower bands and treat each sub-band independently in the model-based mode beamformer. One can then combine the estimates for each non-overlapping sub-bands together in the inverse Fourier transform to construct the modal arrival structures of a higher resolution pulse. The other option is not to combine the sub-band estimates but treat them individually when constructing the time domain modal arrival structure. The former option has the advantage of giving more accurate travel time estimates, whereas the latter has the advantage of giving more travel time data associated with modes at different frequency bands. Modes at different frequencies sample the ocean slightly differently and may help to improve the resolution maps of the ocean frontal structure in a tomographic inverse analysis. The two options need to be evaluated and compared.

By examining the acoustic data from the individual hydrophones of the VLA, the signal phases were observed to roll linearly or quadratically over each transmission. The phase rolls were observed to be stronger for the 400 Hz signals than for the 224 Hz signals and is consistent with the hypothesis of a Doppler shift induced by ocean currents.

It is therefore useful to examine if the Doppler can be compensated to improve the coherence time of the sound channel.

A simulation study of the effect of the VLA tilt on the performance of the mode beamformer is also warranted. A large syntactic foam subsurface buoy with 2,000 lb buoyancy was used to moor the VLA with an expected tilt of less than one degree. It is useful to examine the degradation of the mode beamformer performance as a function of frequency. Although the results at 224 and 400 Hz may not be significantly affected, future shallow water experiments that will use higher frequencies can benefit from this study. An outstanding question is: At what frequency must the VLA tilt be monitored and what is the desired accuracy? The answer to this will be useful for design purposes.

Improvements in the processed results could have been achieved if the tilt sensors on the VLA had functioned as expected. At 400 Hz, an array tilt of 1.0 will result in a quarter wavelength phase shift in the data across the array aperture of 52.5 meters, severely affecting the results. Statistical estimation was performed on this data set to correct for the lack of tilt information resulting in additional uncertainty variances on the final results.

Another low-cost, simple addition to the experiment configuration would be to increase the number of temperature pods used along the vertical array. Having the increased environmental information along the highly variable shelf-break allowed us to account for the temporal variability when calculating the vertical mode structures.

LIST OF REFERENCES

1. Chiu, C.-S., Lynch, J.F., Gawarkiewicz, G.G., Pickart, R.S., Sperry, B., Miller, J.H., Smith, K.B., and Robinson, A.R., "Measurement and Analysis of the Propagation of Sound from the Continental Slope to the Continental Shelf," *J. Acoustic Society of America*, 102(5.2), p.3143, 1997.

2. Lynch, J.F., Gawarkiewicz, G.G., Chiu, C.-S., Pickart, R.S., Miller, J.H., Smith, K.B., Robinson, A., Brink, K., Beardsley, R., Sperry, B., and Potty, G., "Shelfbreak PRIMER - An Integrated Acoustic and Oceanographic Field Study in the Mid-Atlantic Bight," *Shallow Water Acoustics* (R.H. Zhang and J.X. Zhou ed.), China Ocean Press, pp.205-210, 1997.

3. Apel, J., Badiey, M., Chiu, C.-S., Finnette, S., Headrick, R., Kemp, J., Lynch, J., Newhall, A., Orr, M., Paseward, B., Tielbuerger, D., Turgut, A., von der Height, K., Wolf, S., "An Overview of the 1995 SWARM Shallow Water Internal Wave Acoustic Scattering Experiment," *IEEE J. Oceanic Engineering*, 22(3), pp. 465-500, 1997.

4. Chiu, C.-S., Ng, S.-L., and Denner, W.W., "Estimating the Properties of the Sound Field in a Shelf Region Near the Shelfbreak," *Proceedings of the 6th Western Pacific Regional Acoustics Conference*, pp. 329-334, 1997.

5. Chiu, C.-S., Miller, J.H., Denner, W.W., and Lynch, J.F., "Forward Modeling of the Barents Sea Tomography Vertical Line Array Data and Inversion Highlights," in *Full Field Inversion Methods in Ocean and Seismic Acoustics* (O. Diachok, A. Caiti, P. Gerstoft and H. Schmidt editors), Kluwer Academic Publishers, pp. 237-242, 1995.

6. Chiu, C.-S., Miller, J.H., and Lynch, J.F., "Forward Coupled-mode Propagation Modeling for Coastal Ocean Acoustic Tomography," *J. Acoustic Soc. of America*, 99(2), pp. 793-802, 1996.

7. Baggeroer, A.B., Sperry B., Lashkari, K., Chiu, C.-S., Miller, J.H., Mikhalevsky, P.N., and von der Heydt, K., "Vertical Array Receptions of the Heard Island Feasibility Transmissions," *J. Acoustic Soc. of America*, 96(4), pp. 2395-2413, 1994.

8. Medwin, H., and Clay, C.S., *Fundamentals of Acoustical Oceanography*, Chapter 11, Academic Press, San Diego, 1998.

9. Chiu, C.-S., Miller, C. W., and Lynch, J. F., "Optimal Modal Beamforming of Bandpass Signals Using an Undersized Sparse Vertical Hydrophone Array: Theory and a Shallow-Water Experiment," *IEEE Journal of Oceanic Engineering*, Vol. 22, No. 3, pp. 522-533, July 1997.

10. Spindel, R.C., "An Underwater Acoustic Pulse Compression System," *IEEE Transactions on Acoustics, Speech, and Signal Processing*, Vol. ASSP-27, No. 6, December 1979.

11. Birdsall, T. G., Metzger, K., "Factor Inverse Matched Filtering," *J. Acoustic Society of America*, 79(1), pp. 91-99, 1986.

12. Munk, W., Worcester, P., Wunsch, C., *Ocean Acoustic Tomography*, Cambridge University Press, New York, NY, 1995.

13. Ziemer, R. and Peterson, R., *Digital Communications and Spread Spectrum Systems*, Macmillan Publishing Comany, New York, NY, 1985.

14. Chiu, C.-S., Semtner, A.J., Ort, C.M., Miller, J.H., and Ehret, L.L., "A ray variability analysis of sound transmission from Heard Island to California," *J. Acoustic Society of America*, 96(1), pp. 2380-2388, October 1994.

15. Therrien, C. W., *Discrete Random Signals and Statistical Signal Processing*, pp. 528-532, Prentice Hall, Inc., Englewood Cliffs, NJ, 1992.

16. Strang, G., *Linear Algebra and its Applications*, pp. 442-449, Harcourt Brace Jovanovich, Inc., Orlando, FL, 1988.

17. Chiu, C.-S., Miller, J. H., and Lynch, J. F., "Inverse techniques for coastal acoustic tomography," in *Environmental Acoustics*, D. Lee and M. Schultz, Eds. World Scientific, 1994, pp. 917-931.

18. Scharf, L.L., *Statistical Signal Processing: Detection, Estimation, and Time Series Analysis*, Addison-Wesley, Reading, MA, 1991.

INITIAL DISTRIBUTION LIST

No. Copies

1. Defense Technical Information Center 2
   8725 John J. Kingman Rd., STE 0944
   Ft. Belvoir, VA 22060-6218

2. Dudley Knox Library 2
   Naval Postgraduate School
   411 Dyer Rd.
   Monterey, CA 93943-5101

3. Chairman, Code EC 1
   Department of Electrical and Computer Engineering
   Naval Postgraduate School
   833 Dyer Road, Room 437
   Monterey, CA 93943-5121

4. Chairman, Code OC 1
   Department of Oceanography
   Naval Postgraduate School
   833 Dyer Road, Room 324
   Monterey, CA 93943-5122

5. Dr. Ching-Sang Chiu (Code OC/Ci) 2
   Department of Oceanography
   Naval Postgraduate School
   833 Dyer Rd., Room 318
   Monterey, CA 93943-5122

6. Dr. Charles Therrien (Code EC/Ti) 1
   Department of Electrical and Computer Engineering
   Naval Postgraduate School
   833 Dyer Rd., Room 437
   Monterey, CA 93943-5121

7. Mr. Chris Miller (Code UW/Mr) 1
   Department of Undersea Warfare
   Naval Postgraduate School
   589 Dyer Rd., Room 200A
   Monterey, CA 93943-5126

8. Dr. Steve Ramp (Code OC/Ra) 1
Department of Oceanography
Naval Postgraduate School
833 Dyer Rd., Room 318
Monterey, CA 93943-5122

9. Dr. James F. Lynch 1
Department of Applied Physics and Ocean Engineering
Mail Stop #21
Woods Hole Oceanographic Institution
Woods Hole, MA 02543-1047

10. Dr. Jeff Simmen (Code 3210A) 1
Office of Naval Research
800 North Quincy Street
Arlington, VA 22217

11. Dr. Ellen Livingston, Code 3210A 1
Office of Naval Research
800 North Quincy Street
Arlington, VA 22217

12. Dr. Lou Goodman, Code 322PO 1
Office of Naval Research
800 North Quincy Street
Arlington, VA 22217